Available online at www.sciencedirect.com

ScienceDirect

IFAC Papers Online CONFERENCE PAPER ARCHIVE

IFAC-PapersOnLine 48-2 (2015) 274–280

Pool testing of AUV visual servoing for autonomous inspection

Szymon Krupinski * **Remi Desouche** * **Narcis Palomeras** **
Guillaume Allibert *** **Minh-Duc Hua** ****

* *Cybernetix, a Technip company, Marseille, France (email: {szymon.krupinski,remi.desouche}@cybernetix.fr)*
** *Underwater Vision and Robotics Research Center, Girona, Spain (email: npalomeras@silver.udg.edu)*
*** *Laboratoire d'Informatique, Signaux et Systèmes de Sophia-Antipolis, France (email: allibert@i3s.unice.fr)*
**** *Institute des Systèmes Intelligents et de Robotique, Paris, France (email: hua@isir.upmc.fr)*

Abstract: Servoing methods were developed to enable inspection of underwater structures by autonomous vehicles in industrial oil & gas context. Pipeline following and planar object tracking were targeted, using video camera as the principal sensor. A non-linear inner-loop control was used to stabilise the complex dynamics of the vehicle. Pipeline following and planar target tracking were successfully tested in October and November 2014 on Girona 500 vehicle in a simple pool mock-up environment.

Keywords: Autonomous underwater vehicle, image-based visual servoing, non-linear control

1. INTRODUCTION

1.1 Autonomous inspection – objectives

Remotely operated underwater vehicles (ROVs) perform the task of visual inspection of deep-sea infrastructure. Their operations are, however, hampered by the presence of tether, pilot fatigue and the cost of the surface support. Autonomous underwater vehicles (AUVs) have proven their value in simpler operations like bathymetric survey. It is thus a logical step to propose the development of autonomous visual inspection.

The sea water medium is mostly opaque to almost all of the electromagnetic wave spectrum, preventing global GPS-like localisation underwater. Servoing on the basis of the sensor data reflecting the nearest environment can replace it for precise navigation around structures. Acoustic sensors present specific problems, especially in cluttered environments. A video camera is an easily available sensor that provides high-frequency and information-rich data. It has lead to application of visual servoing methods to control an AUV. Position-based methods try to calculate the 3-D pose of the vehicle in its environment and provide an appropriate controller that uses the carthesian information to drive the vehicle to the desired position. Estimation of depth in the image tends to be unreliable. In image-based methods (Espiau et al., 1992), the position controller takes image feature data as its main input. Rives and Borrelly (1997) proposes a feedback-linearising control scheme to visually track a pipeline. Lots et al. (2000) develops a planar homography-based kinematic stabilisation of the vehicle above the sea bottom. While this work brings interesting results, including experimental validation, certain issues are open to improvement, such as the choice of the parameters to estimate or the handling of the complex dynamics of the vehicle. Such improvements were proposed in a series of publications: Krupinski et al. (2012), Hua et al. (2013). These publications present a two-tiered control scheme with a common pilot controller, which can be applied to any servoing solution, not necessarily based on vision. The following article presents the results of experimental validation of the aforementioned theoretical work.

In the sequel, two autonomous tasks are discussed, selected on the basis of their ubiquity in the typical oil & gas inspection operations:

Task 1: Pipeline or cable following During the pipe following task, the vehicle is expected to detect a pipeline in the field of view of its camera and align itself with it. The inspection is performed when the vehicle advances at a predefined reference velocity along the pipe, while regulating its transversal position to match the desired relative position with respect to the pipe center. The heading of the vehicle is usually required to coincide with the orientation of the pipe, since it leads to the optimal motion economy.

Task 2: Structure inspection - stabilisation and structure-relative servoing It will be assumed that the vehicle finds itself in the vicinity of the structure which is the target of inspection and that some part of the structure containing a planar visual target is visible. During a typical

Guillaume Allibert and Minh Duc Hua are supported by the PEPS-CNRS CONGRE project.

Peer review under responsibility of International Federation of Automatic Control.
10.1016/j.ifacol.2015.06.045

inspection task, the vehicle is actuated in order to pass through certain characteristic waypoints around a given structure. It can be defined as a series of stabilisation tasks, where the vehicle is required to move to a reference pose with respect to an object in the visual field of the camera, given a reference image or image point coordinates taken at this pose.

The two tasks above require regulation of the vehicle's position. However, AUVs can usually only be controlled by assigning thruster output and control fin position (in case of underactuated ones). This discrepancy is solved by exploiting the cascade structure of the AUV's dynamics: the control is divided into the **inner loop**, which regulates the velocity of the system to the desired setpoint using the force input (pilot control), and the **outer loop**, which calculates the velocity setpoint necessary to reach the desired position (kinematic control). The timescale separation, with the rapidly converging inner loop, assures the overal stability of the system. The complete architecture of control is presented in Fig. 1.

The vehicle concerned in the development of the control laws was assumed to be fully-actuated. However, care has been taken that the final control scheme be also applicable to hover-capable AUVs, i.e. those which cannot actively control their pitch and roll.

1.2 Vehicle dynamics and inner-loop control

The kinematics and the dynamics of the vehicle was modelled in a mobile frame of reference attached to the AUV's centre of buoyancy. For simplicity, it is assumed that the camera is also attached at the same point and the mobile reference frame is denoted $\mathcal{C}$. The formulation of dynamics is similar to Leonard (1997), with the angular and linear dynamics presented separately. The model and the specific assumptions are introduced in Krupinski et al. (2012). It visually differs from the most commonly used naval architecture notation (cf. Fossen (2002)) but it is mathematically equivalent. The use of rotation matrix $\mathbf{R}$ to represent the orientation of $\mathcal{C}$ in the inertial reference system $\mathcal{A}$ renders it robust against the gimbal lock problem and allows to formulate the controller in a purely algebraic form, avoiding trigonometric functions and their domain limitations.

$$\begin{aligned}\mathbf{M}\dot{\mathbf{V}} - \mathbf{D}\dot{\boldsymbol{\Omega}} &= (\mathbf{M}\mathbf{V} - \mathbf{D}\boldsymbol{\Omega}) \times \boldsymbol{\Omega} + \mathbf{F}_G(\mathbf{R}) + \mathbf{F}_D(\mathbf{V}) + \mathbf{F}_C \\ \mathbf{I}\dot{\boldsymbol{\Omega}} + \mathbf{D}\dot{\mathbf{V}} &= (\mathbf{I}\boldsymbol{\Omega}) \times \boldsymbol{\Omega} + (\mathbf{M}\mathbf{V}) \times \mathbf{V} + \mathbf{D}(\mathbf{V} \times \boldsymbol{\Omega}) \\ &\quad + \mathbf{T}_G(\mathbf{R}) + \mathbf{T}_D(\boldsymbol{\Omega}) + \mathbf{T}_C \end{aligned} \quad (1)$$

In the above model, the symbols $\mathbf{M} := m\mathbf{I}_{3\times 3} + \mathbf{M}_A$ and $\mathbf{I} := \mathbf{I}_0 + \mathbf{I}_A$ represent vehicle's total mass and and inertia matrices. They are constituted by augmenting the mechanical parameters of mass (m) and inertia ($\mathbf{I}_0$) by their hydrodynamic added mass and inertia counterparts - $\mathbf{M}_A$ and $\mathbf{I}_A$ respectively. $\mathbf{D}$ is the crossterm matrix, affected by the distance between the centres of buoyancy and mass of the vehicle r_b. $\mathbf{V}$ and $\boldsymbol{\Omega}$ denote the linear and angular velocities, respectively. $\mathbf{F}$ and $\mathbf{T}$ stand for force and torque. Variables indexed with D correspond to the damping terms due to hydrodynamic effects, while index C denotes the input variables. Index G marks the force and torque created by buoyancy and Earth's gravity.

A pilot controller is developed that drives the system velocities $\mathbf{V}$ and $\boldsymbol{\Omega}$ to the corresponding reference values $\mathbf{V}_r$ and $\boldsymbol{\Omega}_r$. They are to be defined by the outer loop control and are assumed to be bounded. It is equivalent to reducing the following error variables to zero: $\widetilde{\mathbf{V}} := \mathbf{V} - \mathbf{V}_r$ and $\widetilde{\boldsymbol{\Omega}} := \boldsymbol{\Omega} - \boldsymbol{\Omega}_r$. In order to eliminate steady state errors due to discrepancies between the model and reality, additional integrator terms were introduced: $\bar{\mathbf{V}} := \widetilde{\mathbf{V}} + k_{iV}\mathbf{z}_V$, $\bar{\boldsymbol{\Omega}} := \widetilde{\boldsymbol{\Omega}} + k_{i\Omega}\mathbf{z}_\Omega$. $\mathbf{z}_V$ and $\mathbf{z}_\Omega$ are variables representing the output of an integrator over the velocity error equipped with an appropriate anti-windup mechanism and k_{iV} and $k_{i\Omega}$ are positive integral gains. The total control goal is now equivalent to the stabilisation of $(\bar{\mathbf{V}}, \bar{\boldsymbol{\Omega}})$ about zero. The dynamics exposed in Eq. (1) must therefore rewritten in terms of $\bar{\mathbf{V}}$ and $\bar{\boldsymbol{\Omega}}$.

To control this dynamics, the following inner-loop controller is proposed:

$$\begin{cases} \mathbf{F}_C = -\operatorname{sat}_{\boldsymbol{\Delta}_V}(\mathbf{K}_V\bar{\mathbf{V}}) - (\mathbf{M}\bar{\mathbf{V}})_\times\boldsymbol{\Omega}_r + \mathbf{M}^\top(\bar{\boldsymbol{\Omega}}_\times\mathbf{V}_r) \\ \qquad - \bar{\boldsymbol{\Omega}} \times (\mathbf{D}\boldsymbol{\Omega}_r) - \mathbf{F}_G(\mathbf{R}) - \mathbf{F}_D(\mathbf{V}_r) - \bar{\mathbf{F}}_r \\ \mathbf{T}_C = -\operatorname{sat}_{\boldsymbol{\Delta}_\Omega}(\mathbf{K}_\Omega\bar{\boldsymbol{\Omega}}) - (\mathbf{I}\bar{\boldsymbol{\Omega}})_\times\boldsymbol{\Omega}_r + (\mathbf{D}\bar{\boldsymbol{\Omega}})_\times\mathbf{V}_r - \mathbf{T}_D(\boldsymbol{\Omega}_r) - \bar{\mathbf{T}}_r \end{cases}$$

where a canonical saturation function $sat()$ was introduced to ensure that the control input does not exceed the capacity of the actuators. The variables $\bar{\mathbf{F}}_r$ and $\bar{\mathbf{T}}_r$ contain the terms involving the derivative of the reference velocities $\dot{\mathbf{V}}_r$ and $\dot{\boldsymbol{\Omega}}_r$. These quantities must therefore be computable in order to calculate the control force and torque $\mathbf{F}_C$ and $\mathbf{T}_C$. It is thus left to the outer loop control to furnish the reference velocity and its derivative. The gravity-buoyancy torque $\mathbf{T}_G(\mathbf{R})$ does not need to be compensated in the controller, as it is a natural stabilisation feature of the vehicle. The angular velocity and orientation can be estimated by a gyro or an inertial measurement unit, while the linear velocity is measured by the Doppler velocity log.

The proof of the stability of the proposed controller can be performed by considering the following Lyapunov function candidate:

$$\mathcal{L}_i = \frac{1}{2}\left(\widetilde{\mathbf{V}}^\top\mathbf{M}\widetilde{\mathbf{V}} + \widetilde{\boldsymbol{\Omega}}^\top\mathbf{I}\widetilde{\boldsymbol{\Omega}}\right) - \widetilde{\mathbf{V}}^\top\mathbf{D}\widetilde{\boldsymbol{\Omega}} + mgl\widetilde{\boldsymbol{\Omega}}^\top\mathbf{e}_3 \times \mathbf{R}^\top\mathbf{e}_3$$

and its derivative

$$\dot{\mathcal{L}}_i = \widetilde{\mathbf{V}}^\top(\mathbf{M}\dot{\widetilde{\mathbf{V}}} - \mathbf{D}\dot{\widetilde{\boldsymbol{\Omega}}}) + \widetilde{\boldsymbol{\Omega}}^\top(\mathbf{I}\dot{\widetilde{\boldsymbol{\Omega}}} + \mathbf{D}\dot{\widetilde{\mathbf{V}}}) - mgl\boldsymbol{\Omega}^\top\mathbf{e}_3 \times \mathbf{R}^\top\mathbf{e}_3\,.$$

where the term $mgl\widetilde{\boldsymbol{\Omega}}^\top\mathbf{e}_3 \times \mathbf{R}^\top\mathbf{e}_3$ represents the potential energy of gravitation when the vehicle is rolled or pitched away from its stable orientation. l is the leaver arm between the vehicle mass and buoyancy centres and $\mathbf{e}_3$ is the vector pointing towards the bottom of the vehicle.

1.3 Visual servoing for pipeline following

This section describes the visual servo control in order to perform autonomous pipeline following introduced in details in Krupinski et al. (2012). The visual features considered are the pipeline borders assumed to be parallel to each other (see Fig. 2). The unit direction vector of the pipeline, specified up to a sign, is denoted as $\mathbf{u}$ when expressed in the inertial frame $\mathcal{A}$ and as $\mathbf{U} = [U_1\ U_2\ U_3]^\top$ when expressed in the camera frame $\mathcal{C}$. One verifies that $\mathbf{U} = \mathbf{R}^\top\mathbf{u}$. A position-like and yaw-related error terms will be derived from the visual features. The first one is based on the bi-normalized Plücker coordinates of the observed parallel lines and is used to align the camera at a desired

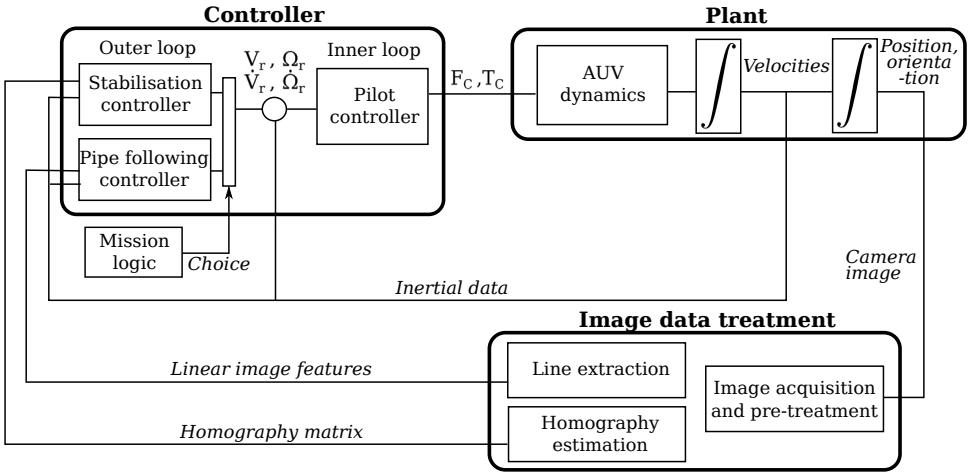

Fig. 1. Diagram of the control scheme, showing the interconnections of the inner and outer loop controllers.

distance with respect to the pipeline.

In the original normalized Pluecker line coordinates, vector $\mathbf{P} \in \mathcal{C}$ connects the camera's image centre with the closes point on the line l. Thus, $\mathbf{P} \perp \mathbf{U}$. Define $\mathbf{H} \in \mathcal{C}$ as:

$$\mathbf{H} = \mathbf{P} \times \mathbf{U}\,. \tag{3}$$

Then, the pair $(\mathbf{H}, \mathbf{U})$ defines a unique line in space. If $\mathbf{H}$ is normalised as $\mathbf{h} := \frac{\mathbf{H}}{|\mathbf{H}|}$, $(\mathbf{h}, \mathbf{U})$ will define a family of parallel lines. These coordinates, expressed in the camera frame $\mathcal{C}$, can be measured directly from the image features. One can propose a centroid vector computed from the image features $(\mathbf{h}_1, \mathbf{h}_2)$ of two parallel lines as follows:

$$\mathbf{q} := \mathbf{h}_1 + \mathbf{h}_2.$$

The visual position error with respect to the linear borders of the pipeline can then be defined as:

$$\boldsymbol{\delta}_1 = \mathbf{q}^* - \mathbf{q}\,,$$

where $\mathbf{q}^*$ is the value of the q vector for a reference configuration of the features. It is considered as constant in $\mathcal{A}$. The error variable $\boldsymbol{\delta}_1$ contains enough information about the lateral position of the vehicle (or, to be precise, the camera) above the pipeline that it could be used to formulate a simple law of control inspired by Mahony and Hamel (2005).

$$\mathbf{V} := k_\delta \mathbf{U} \times \boldsymbol{\delta}_1 + v_r \mathbf{U}\,,$$

with v_r, the desired velocity of advance along the pipe and a positive constant k_δ.

However, in the expression of $\dot{\mathbf{V}}$ one will find the depth of the image features $|\mathbf{H}|$ which is unmeasurable in the image, making the derivative of the reference velocity unknown. The proposed visual servo control is thus based on another error variable, $\boldsymbol{\delta}_2$, which is defined by its derivative:

$$\dot{\boldsymbol{\delta}}_2 := -\boldsymbol{\Omega} \times \boldsymbol{\delta}_2 - k_1 \boldsymbol{\delta}_2 + k_2 \boldsymbol{\delta}_1,\ \boldsymbol{\delta}_2(0) = \boldsymbol{\delta}_1(0),\ k_{1,2} > 0$$

Note that $\boldsymbol{\delta}_2$ is a simple filter on $\boldsymbol{\delta}_1$ and that at any time its value and its time-derivative $\dot{\boldsymbol{\delta}}_2$ are known. It can be shown that $\boldsymbol{\delta}_2$ preserves the property of $\boldsymbol{\delta}_1$ of being orthogonal to $\mathbf{U}$.

The reference translational velocity of the camera $\mathbf{V}_{Cr}$ can then be defined as

$$\mathbf{V}_{Cr} := k_\delta \mathbf{U} \times \boldsymbol{\delta}_2 + v_r \mathbf{U}\,, k_\delta > 0\,. \tag{4}$$

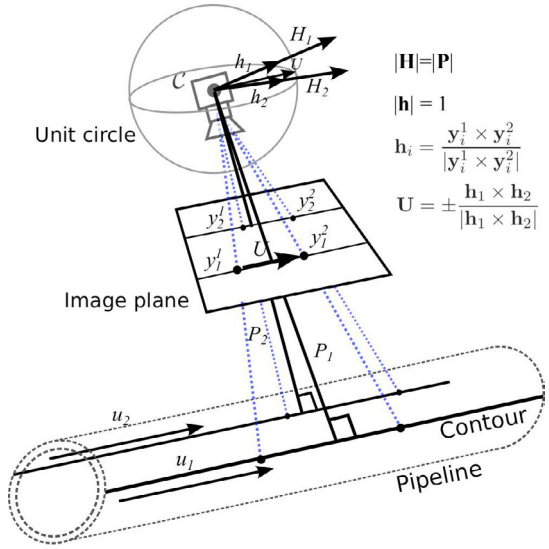

Fig. 2. Geometrical representation of the error variables based on binormalised Pluecker coordinates used for pipeline following. The algebraic recovery of the servoing variables directly from the image is illustrated.

The proof of stability of this part of the outer controller can be found by analysing the dynamics of the error system $(\dot{\boldsymbol{\delta}}_1, \dot{\boldsymbol{\delta}}_2)$ using singular perturbation theorem. The part of the visual error dynamics coming from the vehicle dynamics can be assumed to be a singular perturbation, as it is quickly brought to zero by the inner loop control. Finally, the reference angular velocity is defined as

$$\boldsymbol{\Omega}_r := k_U U_2 \mathbf{e_3},\ k_U > 0\,, \tag{5}$$

with U_2 the y-axis component of the $\mathbf{U}$ vector. The stability of this scheme can be demonstrated by looking at the Lyapunov candidate function $\mathcal{L}_u := 1 - \mathbf{U}^\top \mathbf{e_1}$ and its derivative $\dot{\mathcal{L}}_u = \mathbf{U}^\top \boldsymbol{\Omega}_\times \mathbf{e_1} = \boldsymbol{\Omega}^\top (\mathbf{e_1} \times \mathbf{U}) = -k_u U_2^2$, where $\mathbf{e_1}$ is the unit vector pointing to vehicle's nose.

1.4 Visual stabilisation

In this section, another controller, introduced in details in Hua et al. (2013), is presented in order to perform the task of stabilisation of the AUV in relation to a visual target viewed by its camera. A reference image of a planar target

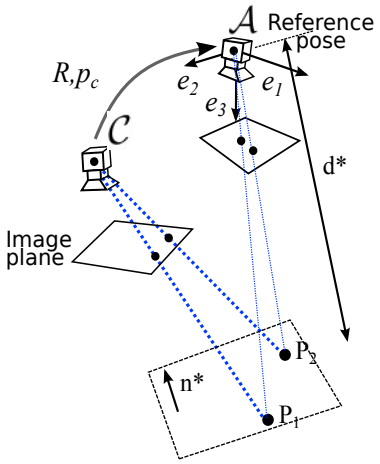

Fig. 3. Geometrical representation of the planar homography used for visual stabilisation.

(i.e. object to be tracked) is taken at some desired pose (i.e. position and orientation) represented by the inertial frame $\mathcal{A}$. Based on this reference image and the current image, the control objective consists in stabilising the pose of the camera to this desired pose. Assume that the camera provides the measurement of the homography matrix $\mathbf{M}_H$ which contains all transformation information between two images of the same planar object of interest, where $\mathbf{M}_H$ is given by Benhimane and Malis (2007):

$$\mathbf{M}_H = \mathbf{R}_C^\top - \frac{1}{d^*}\mathbf{R}_C^\top \mathbf{p}_C \mathbf{n}^{*\top},$$

where d^* is the distance between the target plane and the camera optical center, and $\mathbf{n}^* = [n_1^* \quad n_2^* \quad n_3^*]^\top$ is the unit vector normal to the target plane, expressed in the inertial frame $\mathcal{A}$. The inter-image rotation and displacement of $\mathcal{C}$ is illustrated in Fig. 3. Note that $\mathbf{R}_C \equiv \mathbf{R}$ is used to simplify the presentation.

Homography matrix can be estimated directly by the visual sensor. Control design difficulties lie in the fact that d^* and $\mathbf{n}^*$ are unknown and that $\mathbf{M}_H$ only contains a coupled information of rotation and translation. One can, however, base a kinematic control directly on $\mathbf{M}_H$, as proposed in (Benhimane and Malis, 2007). Let $\mathbf{e}_p, \mathbf{e}_\Theta \in \mathbb{R}^3$ denote the error vectors defined as:

$$\mathbf{e}_p := (\mathbf{I}_3 - \mathbf{M}_H)\mathbf{m}^*, \quad \mathbf{e}_\Theta := \text{vex}(\mathbf{M}_H^\top - \mathbf{M}_H),$$

with some arbitrary unit vector $\mathbf{m}^* \in \mathbb{S}^2$ approximating the normal vector of the target plane. Then, the following kinematic control law can be shown to stabilise the camera around $(\mathbf{R}, \mathbf{p}_c) = (\mathbf{0}, \mathbf{0})$:

$$\mathbf{V}_C = -\lambda_p \mathbf{e}_p\,, \quad \boldsymbol{\Omega} = -\lambda_\Theta \mathbf{e}_\Theta,$$

with $\lambda_p, \lambda_\Theta$ some positive gains.

The above formulation cannot be directly adopted for the AUV inspection task for several reasons. Firstly, analysis shows that the derivative of $\mathbf{e}_p$ cannot be calculated without the feature depth information, thus the derivative of the reference velocity cannot be furnished to the inner-loop controller. Secondly, the orientation servoing uses a full vector of control torque to regulate the orientation, while in a practical vehicle yaw is typically the only fully-actionned d.o.f. in orientation. The following augmented system is proposed which includes a new variable $\mathbf{z}_p$

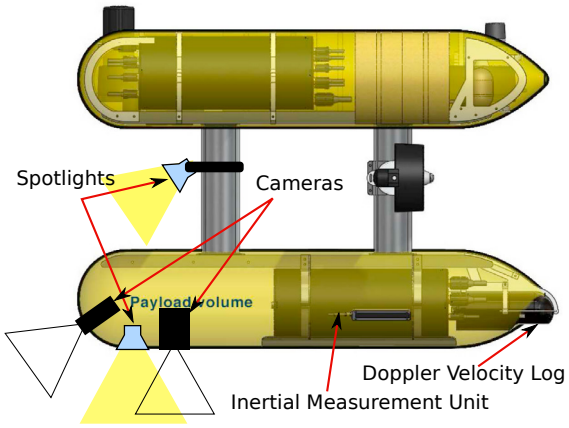

Fig. 4. Test vehicle configuration and sensors used for servoing. Only one camera of the two would be used at any time.

encapsulating the knowledge of the depth of the features without explicitly calculating them:

$$\begin{cases} \dot{\mathbf{z}}_p = -\boldsymbol{\Omega}_r \times \text{sat}_\nabla(\mathbf{e}_p) - k_z(\mathbf{z}_p - \text{sat}_\Delta(\mathbf{z}_p)),\ \mathbf{z}_p(0) = \mathbf{0} \\ \dot{\hat{\mathbf{e}}}_p = -\boldsymbol{\Omega} \times \hat{\mathbf{e}}_p - k_2(\hat{\mathbf{e}}_p - \mathbf{e}_p),\ \hat{\mathbf{e}}_p(0) = \mathbf{e}_p(0) \end{cases}$$

where Δ and ∇ are saturation bounds large enough to assure the stability of the observer scheme. Consider the following reference translational velocity:

$$\mathbf{V}_{Cr} := -k_1 \hat{\mathbf{e}}_p - \boldsymbol{\Omega}_r \times \mathbf{z}_p \tag{6}$$

where k_1 and k_2 are appropriately chosen scalar gains.

The design of the yaw control will be based on the observation that $\mathbf{R}\mathbf{e}_3$ (almost) globally converges to $\mathbf{e}_3$, that guarantees the convergence of $\mathbf{R}$ to $\mathbf{R}_\psi$ defined by:

$$\mathbf{R}_\psi := \begin{bmatrix} \cos\psi & -\sin\psi & 0 \\ \sin\psi & \cos\psi & 0 \\ 0 & 0 & 1 \end{bmatrix}.$$

Using an off-diagonal element of the matrix $\mathbf{M}_H$, $M_{H\{1,2\}}$, the reference angular velocity can be defined as $\boldsymbol{\Omega}_\mathbf{r} := \omega_{3r}\mathbf{e}_3 + k_\omega \mathbf{e}_3 \times \mathbf{R}^\top \mathbf{e}_3$, where ω_{3r} is the solution of the following equation:

$$\dot{\omega}_{3r} := -k_4\omega_{3r} - k_3 \text{sat}^{\Delta_\omega}(M_{H\{1,2\}}), \quad \omega_{3r}(0) = 0, \tag{7}$$

with k_3, k_4 some positive gains and $\Delta_\omega > 1$ a saturation bound. For the relatively complex proof of the stabilisation scheme, the reader is referred to Hua et al. (2013).

Having recalled the control scheme details, the sequel of this article focuses on the results obtained during practical tests.

2. TESTING AND RESULTS

2.1 Pool testing setup

The control solution presented in the previous sections in form of controllers (4), (5), (6) and (7) was implemented as Python modules included into a broader ROS package. The vehicle chosen for to carry out the testing was Girona 500 developed by Underwater Vision and Robotics Center in Girona, Spain. It is controlled by COLA2 software system (Palomeras et al., 2012). The AUV was equipped with a PAL forward-looking and a Fire-Wire downward-looking camera, both providing colour images at about 5-7Hz. An electornic gyro and a Doppler velocity log (DLV)

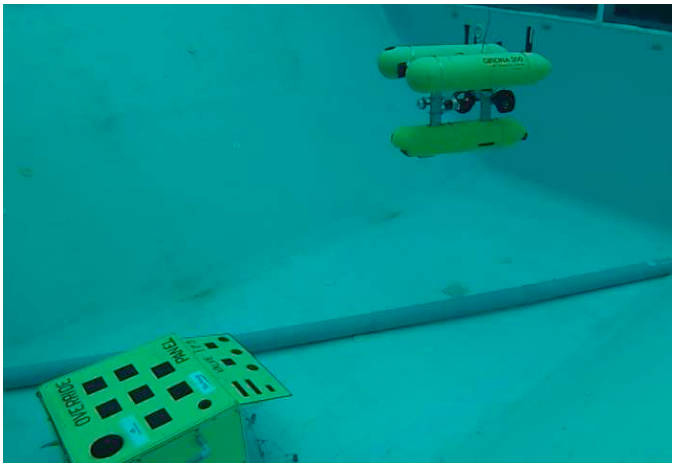

Fig. 5. AUV follows the mock pipeline. The mockup of a subsea manifold to be inspected is also visible in the photo.

were used to measure the velocity of the vehicle. The last sensor could also estimate the altitude of the vehicle above the bottom. Sloping bottom would disturb the signal of the DVL, limiting the space available for the trials.

The inner controller was parametrised using values taken from Karras et al. (2013). While those parameters could not be expected to be exactly true, Girona 500 being a frequently re-configured vehicle, their precise value was not of paramount importance. The non-linear character of the pilot control meant that it had good stability margins. With suitable gain tuning, the inner loop control was quickly found to stabilise the vehicle's dynamics very well. The significant height of the AUV and the lack of means to regulate its roll meant that some pendulum-like motion in this d.o.f. had to be accepted, if the lateral displacement was to be rapid enough.

2.2 Pipeline following

The vehicle was brought to a point where a part of the pipeline was visible and the guidance algorithm was launched. The vehicle aligned its heading with the pipe and centered its position above it, as a consequence of using a horizontal reference vector $q^* = [0.0, 1.96, 0.0]^\top$. The settling of the altitude to within 20 cm of the desired altitude took approximately twice as long. The reference forward velocity of $0.15\frac{m}{s}$ was reached and stabilised almost immediately. Figures 6, 7 and 8 illustrate the input and output of the pipe following controller.

2.3 Stabilisation

The stabilisation was tested by collecting images from one of the two cameras to serve as reference images and selecting the region of interest in which the planar target was present. The vehicle would then be brought to a different position and orientation in which a large part of the same target was visible. The guidance algorithm was then launched and the vehicle converged to the reference position. The servoing was tested using downwards-looking

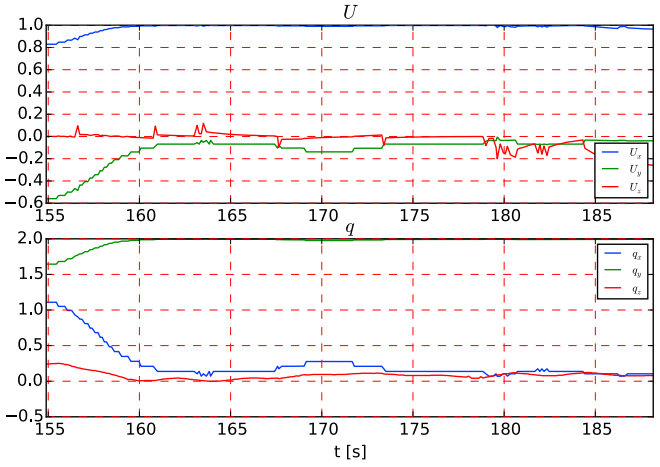

Fig. 6. Error variables U and q representing the pipe direction and transversal position in the AUV reference frame, respectively, during the pipe following exercise. They both quickly converge to and remain around their desired values: $[1.0, 0.0, 0.0]^\top$ and $[0.0, 1.96, 0.0]^\top$ respectively. The errors at t=185 s correspond to the false detections coinciding with the end of the test pipe.

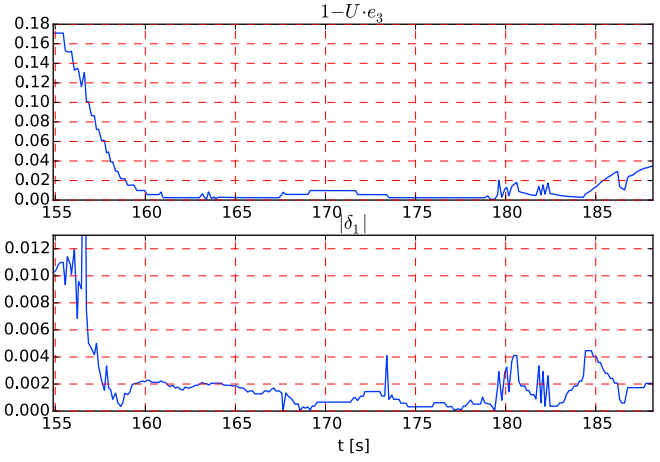

Fig. 7. The convergence rate can be better illustrated by examining the norm of the direction and position error.

and forward-looking camera, thus allowing the top and side portions of the target structure to be used. The test presented in this article used the down-looking camera. The initial and final situation, as seen by the camera, is depicted in Fig. 10. Fig. 12 presents the output of the outer-loop controller and Fig. 13 shows the resulting trajectory and orientation of the AUV. Due to the relatively shallow pool, only a little initial altitude error was introduced. Other tests, for which the target structure was lowered, confirmed that the servoing worked equally well on the horizontal and vertical planes. Due to relatively slow lateral motion of the vehicle, the full convergence took about 40 s.

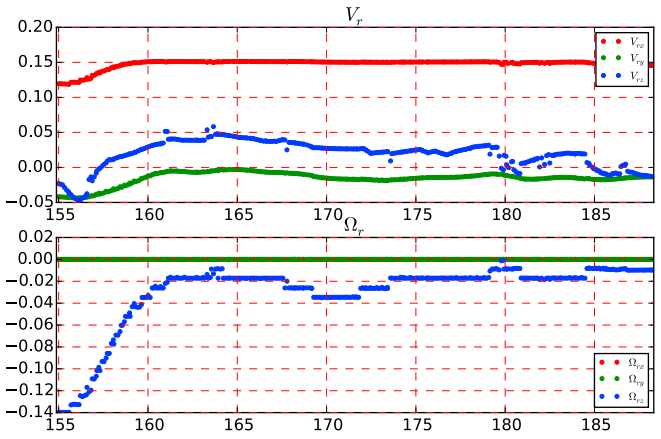

Fig. 8. Reference velocities V_r and Ω_r calculated by the controller corresponding to pipe following test. The reference velocity along the x-axis that quickly converges to 0.15 $\frac{m}{s}$ corresponds to the chosen desired forward velocity v_r.

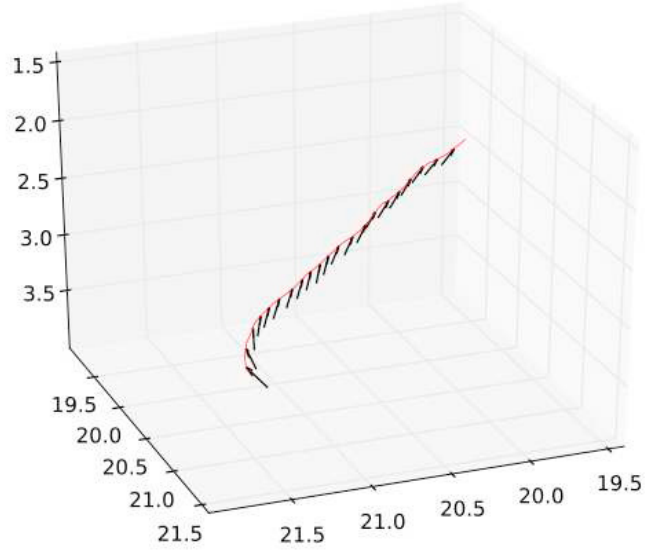

Fig. 9. Vehicle trajectory and orientation during pipeline following calculated using CIRS Unscented Kalman filter methodology. The overall change of depth before stabilising the trajectory is of the order of 1 m.

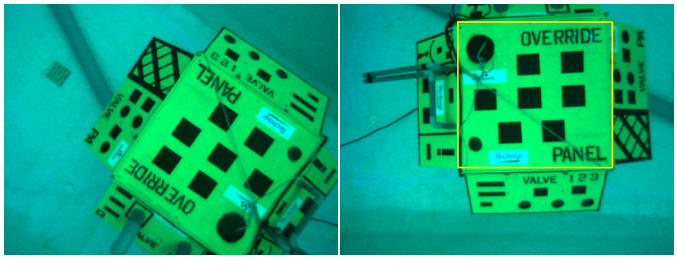

Fig. 10. Initial and final images of the simple stabilisation trial with the down-looking camera. Yellow rectangle marks the planar target of interests, where features are sought to be matched and compared with the reference. The initial heading error is of the order of 160°.

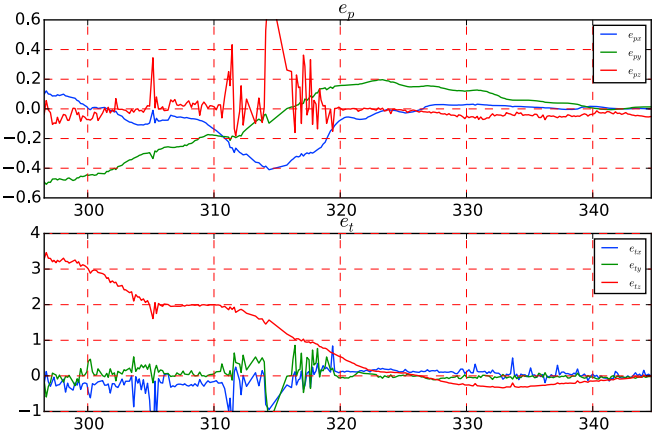

Fig. 11. Visual errors of position ($\mathbf{e}_p$) and orientation ($\mathbf{e}_t$) calculated on the basis of homography matrix. There is a considerable perturbation when the vehicle reaches 90° of its desired orientation: the target was almost lost from the camera's view due to excessive roll of the vehicle.

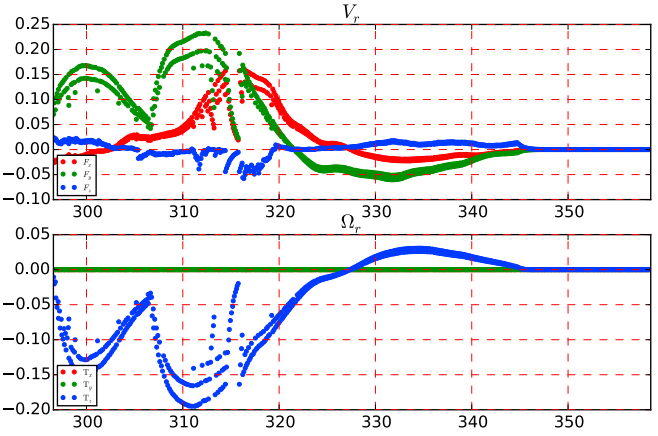

Fig. 12. Reference velocities V_r and Ω_r calculated by the controller corresponding to the stabilisation test. Certain curves seem to be doubled, where in fact the second curve is created by resending values reduced by a fixed factor every time when the image data fails to arrive before 100ms of the last update.

3. CONCLUSIONS AND FURTHER WORK

The tests have validated the theoretical principles of the controller system and confirmed the overall stability of the chosen control architecture. The inner loop control was found to stabilise the vehicle and assure that it attains the desired velocity. The integrator variables have provided smooth buoyancy compensation. The pipeline following was successfull, with the vehicle quickly aligning its trajectory with the mock pipeline and regulating its speed correctly. The tracking of the flat panels of the structure was tested in many configurations, with very positive conclusions regarding the stability and rapidity of operation which outperformed human operators, especially over large initial errors. The test have also led us to improve the image treatment to match the real-world

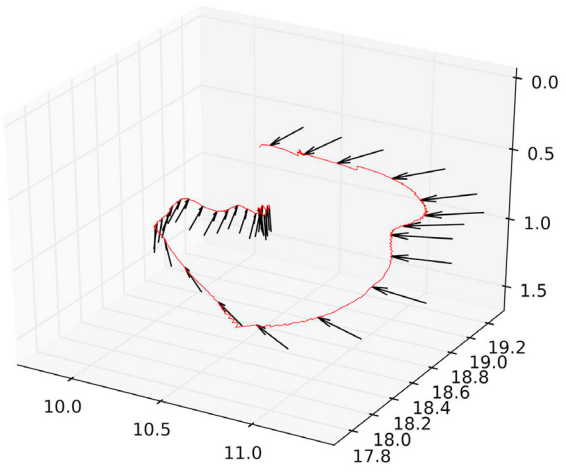

Fig. 13. Vehicle trajectory and orientation during a stabilisation trial. The initial yaw error is close to 180°. This quasi-circular path is traced by the vehicle's center, while the camera stays oriented down on the target.

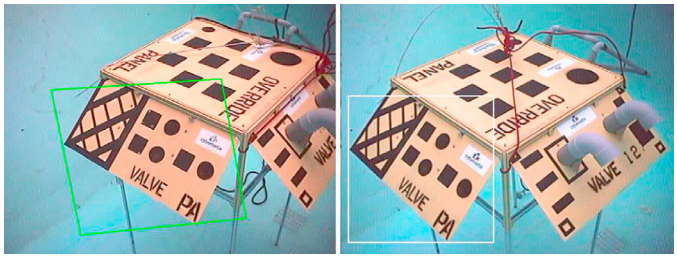

Fig. 14. An example of a stabilisation run using a forward-looking camera.

challenges and to collect valuable data for further research.

In further work, the testing in portuary conditions, viewed as the ultimately hard test case due to high water turbidity and bio-fouling of structures, should be performed.

ACKNOWLEDGEMENTS

We gratefully acknowledge the help of the Girona CIRS team: Pere Ridao, Arnau Carrera, Guillem Vallicrosa, Angelos Mallios, Josep Bosch and Lluís Magí, and thank them for their patience that helped us understand and overcome many problems.

REFERENCES

Benhimane, S. and Malis, E. (2007). Homography-based 2D Visual Tracking and Servoing. *International Journal of Robotics Research*, 26(7), 661–676.

Espiau, B., Chaumette, F., and Rives, P. (1992). A new approach to visual servoing in robotics. 8(3), 313–326.

Fossen, T.I. (2002). *Marine Control Systems*. Marine Cybernetix AS.

Hua, M.D., Allibert, G., Krupinski, S., and Hamel, T. (2014). Homography-based visual servoing for autonomous underwater vehicles. In *IEEE/RSJ International Conference on Intelligent Robots and Systems*, to appear.

Karras, G.C., Bechlioulis, C.P., Leonetti, M., Palomeras, N., Kormushev, P., Kyriakopoulos, K.J., and Caldwell, D.G. (2013). On-line identification of autonomous underwater vehicles through global derivative-free optimization. In *American Control Conference*, 3859–3864.

Krupinski, S., Allibert, G., Hua, M.D., and Hamel, T. (2012). Pipeline tracking for fully-actuated autonomous underwater vehicle using visual servo control. In *American Control Conference*, 6196–6202.

Leonard, N.E. (1997). Stability of a bottom-heavy underwater vehicle. *Automatica*, 33(3), 331–246.

Lots, J.F., Lane, D.M., and Trucco, E. (2000). Application of 2 1/2 d visual servoing to underwater vehicle station-keeping. In *MTS/IEEE OCEANS*, volume 2, 1257–1264.

Mahony, R. and Hamel, T. (2005). Image-based visual servo control of aerial robotic systems using linear image features. *IEEE Transactions on Robotics*, 21(2), 227–239.

Palomeras, N., El-Fakdi, A., Carreras, M., and Ridao, P. (2012). COLA2: A Control Architecture for AUVs. *IEEE Journal of Oceanic Engineering*, 37(4), 695–716.

Rives, P. and Borrelly, J.J. (1997). Underwater Pipe Inspection Task using Visual Servoing Techniques. In *IEEE/RSJ International Conference on Intelligent Robots and Systems (IROS)*, 63–68.